Analyst

PAPER

View Article Online
View Journal

Cite this: DOI: 10.1039/c9an02106j

Dual platform based sandwich assay surface-enhanced Raman scattering DNA biosensor for the sensitive detection of food adulteration†

Ibrahim Khalil, [a] Wageeh A. Yehye, *[a] Nurhidayatullaili Muhd Julkapli, [a] Abu Ali Ibn Sina, [b] Shahrooz Rahmati,[a,c,d] Wan Jefrey Basirun[a,e] and Ali Seyfoddin[f,g]

Surface enhanced Raman scattering (SERS) DNA biosensing is an ultrasensitive, selective, and rapid detection technique with the ability to produce molecule-specific distinct fingerprint spectra. It supersedes the long amplicon based PCR assays, the fluorescence and spectroscopic techniques with their quenching and narrow spectral bandwidth, and the electrochemical detection techniques using multiplexing. However, the performance of the SERS DNA biosensor relies on the DNA probe length, platform composition, both the presence and position of Raman tags and the chosen sensing strategy. In this context, we herein report a SERS biosensor based on dual nanoplatforms with a uniquely designed Raman tag (ATTO Rho6G) intercalated short-length DNA probe for the sensitive detection of the pig species *Sus scrofa*. In the design of the signal probe (SP), a Raman tag was incorporated adjacent to the spacer arm, followed by a terminal thiol modifier, which consequently had a strong influence on the SERS signal enhancement. The detection strategy involves the probe–target DNA hybridization mediated coupling of the two platforms, *i.e.*, the graphene oxide-gold nanorod (GO-AuNR) functionalized capture probe (CP) and SP-conjugated gold nanoparticles (AuNPs), consequently enhancing the SERS intensity by both the electromagnetic hot spots generated at the junctions or interstices of the two platforms and the chemical enhancement between the AuNPs and the adsorbed intercalated Raman tag. This dual platform based SERS DNA biosensor exhibited outstanding sensitivity in detecting pork DNA with a limit of detection (LOD) of 100 aM validated with DNA extracted from a pork sample (LOD 1 fM). Moreover, the fabricated SERS biosensor showed outstanding selectivity and specificity for differentiating the DNA sequences of six closely related non-target species from the target DNA sequences with single and three nucleotide base-mismatches. Therefore, the developed short-length DNA linked dual platform based SERS biosensor could replace the less sensitive traditional methods of pork DNA detection and be adopted as a universal detection approach for the qualitative and quantitative detection of DNA from any source.

Received 21st October 2019,
Accepted 1st December 2019

DOI: 10.1039/c9an02106j

rsc.li/analyst

[a]*Nanotechnology & Catalysis Research Centre (NANOCAT), Institute for Advanced Studies (IAS), University of Malaya, Kuala Lumpur 50603, Malaysia. E-mail: wdabdoub@um.edu.my; Fax: +6037967 6556; Tel: +603 7967 6954*

[b]*Centre for Personalised Nanomedicine, Australian Institute for Bioengineering and Nanotechnology (AIBN), Corner of College and Cooper Roads (Bldg 75), The University of Queensland, Brisbane, QLD 4072, Australia*

[c]*School of Chemistry, Physics and Mechanical Engineering, Science and Engineering Faculty, Queensland University of Technology, Brisbane, Australia*

[d]*Centre for Tropical Crops and Biocommodities, Queensland University of Technology, Brisbane, Australia*

[e]*Department of Chemistry, Faculty of Science, University of Malaya, Kuala Lumpur 50603, Malaysia*

[f]*Drug Delivery Research Group, School of Science, Faculty of Health and Environmental Sciences, Auckland University of Technology, Auckland, New Zealand*

[g]*School of Interprofessional Health Studies, Faculty of Health and Environmental Sciences, Auckland University of Technology, Auckland, New Zealand*

†Electronic supplementary information (ESI) available. See DOI: 10.1039/c9an02106j

Introduction

Meat adulteration is now a matter of great concern due to recent meat scandals that received intense public outrage and global media coverage, consequently leading to huge economic losses.[1–3] Apart from commercial reasons, the adulteration of meat products is a major concern for adverse health effects due to allergies caused by undeclared food ingredients as well as for cultural and religious issues.[4,5] Meat adulteration is typically committed by the substitution of a cheaper meat for a high-value one. Pork, which is one of the most commonly available and globally consumed meats, along with beef and poultry, has similar color and texture to mutton or beef and is generally substituted for these two kinds of meat to pursue higher economic profits.[6,7] Moreover, the halal and kosher

global meat markets are now fast expanding from huge demand for their certified products due to the perception of safety and better quality as well as ethnic considerations.[8,9] Therefore, the development of a sensitive, reliable and rapid pork detection method is in high demand as a first line of defense for detecting and deterring food fraud or accidental cross-contamination, especially in processed meat products, which could assist in preventing unfair business competition, boost consumer confidence and economic growth, and lead to more social harmony.

Different assay techniques, mostly based on protein or DNA biomarkers, have been employed to verify the authenticity of meat products and identify the origin of the species. Pork fat (lard) or protein marker based techniques include high-performance liquid chromatography,[10] electrophoretic methods,[9,11] FTIR, UV-Vis and mass spectroscopies,[12] enzyme-linked immunosorbent assay (ELISA)[13] and the recently developed lateral flow devices.[14] However, the requirements of costly instruments, substantial laboratory setup and specialized skilled personnel for operation and data interpretation, the inability to differentiate closely related species from mixed sample matrices due to cross-species reactions, and, above all, the thermal instability of lipids and proteins have lessened the applicability of these mentioned techniques for both raw and processed food products.[15] In contrast, DNA based detection techniques have shown greater success due to higher stability, specificity, sensitivity and accuracy.[16] Polymerase chain reaction (PCR) based DNA detection methods, such as species-specific PCR,[17] PCR-restriction fragment length polymorphism[15] and real time PCR,[4,16] have been employed for both qualitative and quantitative evaluation of pork residues in meat and meat products. However, the reduction of amplicon length (≤150 bp) in PCR techniques is often challenging, as it reduces the specificity of the technique and produces artifacts in the final result.[18] Hence, different short-length DNA linked nanoparticle based sensing strategies, such as colorimetry,[19] fluorescence spectroscopy,[20] electrochemistry,[21] surface plasmon resonance and SERS techniques, have been considered as promising alternatives to replace the PCR based technique for more sensitive detection.

SERS is a sophisticated approach that enables single molecule identification and is therefore considered as one of the most powerful analytical techniques for DNA detection.[22,23] Recently, we reported a SERS based DNA biosensor that utilized SERS-active dual platforms and co-adsorption of a probe sequence and Raman tag on AuNPs for the sensitive detection of Malayan box turtle (MBT) DNA.[24] However, in spite of the excellent sensitivity, it is difficult to maintain the ratio of the Raman dye and probe sequences on the same nanostructures in the co-adsorption process. Therefore, the preparation of SERS label by an alternative but effective way *via* intercalating the Raman tag in the DNA probe sequences was tested. However, the distance between the intercalated Raman tag and the surface of nanostructured platform has a significant role in the SERS intensity, *i.e.*, the closer the Raman tag the greater the amplification, hence the improved sensitivity.[25,26] There are a few factors that influence the performance of the SERS sensing system, such as electromagnetic enhancement induced by the nanoparticle aggregated hot spots, chemical enhancement dependent on the distance between the Raman tag and the surface of the corresponding nanoparticles, as well as the structure, shape, arrangement and composition of the sensing platform.[27] Hence, the SERS DNA biosensor adopting a novel design intercalating the Raman tag with the DNA probe sequences and the dual platform based sandwich assay technique could be the strategy to achieve greater sensitivity due to the enhanced SERS signal.

Herein, we report a novel SERS DNA biosensing strategy based on the self-assembly of two platforms *via* probe–target hybridization for the trace sensing of pork DNA. In this sensing strategy, GO-AuNR and AuNP were used as the platform while a uniquely designed DNA probe sequence intercalating ATTO Rho6G was used as the signal probe DNA. The ATTO Rho6G was intercalated in such a way that upon the attachment of the SP sequence, the intercalated Raman tag had a position closer to the AuNPs surface while the nucleotide bases remained independent for hybridization. Therefore, the hybridization of the target DNA with the corresponding two split-probe DNA functionalized onto two different platforms facilitates the covalent coupling of the AuNPs over GO-AuNRs and enhances the local electromagnetic field due to the 'hot spots' originating between the GO-AuNR and AuNP systems.[28,29] Moreover, the GO-AuNR nanocomposite itself also contributes to SERS enhancement owing to its stronger inherent light scattering properties, the electron transfer ability of AuNRs, and the synergistic effect of the two individual components.[30] With this approach, the higher the target DNA concentration, the more coupling of the two platforms occurs, which consequently leads to a more intense SERS signal. Therefore, with greater amplification of the SERS signal, even a very low concentration of pork DNA (100 aM) was detected. Moreover, due to the very short-length DNA probe sequences, the fabricated biosensor showed excellent sequence specificity and sensitivity to distinguish the DNA sequences of six closely relevant non-target species from target DNA with single-base mismatch. This is a straightforward, unique, facile and highly specific and sensitive DNA sensing strategy, which could have versatile applications in food safety and security, detection of pathogens, diagnosis of diseases such as cancer, and forensics.

Experimental

Synthesis of GO, AuNPs, AuNRs and GO-AuNR composite

Graphene oxide and AuNPs were synthesized as per the protocols described in our previous study[24] and the details are provided in the ESI.† AuNRs were synthesized in aqueous solution following the seed mediated protocol with minor modifications as reported by Feng *et al.*[31] In brief, the seed solution was prepared by mixing CTAB (3.75 mL, 0.1 M) and $HAuCl_4$ solution (50 μL, 24 mM), followed by the addition and mixing

of ice-cold $NaBH_4$ (300 μL, 0.01 M) using slow magnetic stirring for 2 min. The color of the solution changed from yellow to light brown within 1–2 min, indicating the formation of Au seeds. The solution was then kept standing at room temperature for at least 2 h. The growth solution was prepared by mixing $HAuCl_4$ (204 μL, 24 mM), CTAB (10 mL, 0.1 M), H_2SO_4 (200 μL, 0.5 M) and $AgNO_3$ (100 μL, 10 mM) in a flask, followed by a drop-wise slow addition of ascorbic acid until the solution turned colorless (0.1 M, around ~80 μL). Finally, 24 μL of seed solution was added to the growth solution at room temperature to initiate the formation of AuNRs; the color of the solution gradually changed between 10–20 min. The solution was kept standing under the same conditions at room temperature overnight. The as-synthesized AuNRs were washed twice by centrifuging at 11 000 rpm with ultra-pure water (UPW) for 15 min to remove the excess surfactant. Finally the obtained AuNR precipitate was redispersed in UPW and stored at room temperature for routine use. GO-AuNR composite was synthesized *via* the electrostatic self-assembly technique reported by Han *et al.*[32] First, a 0.5 mg mL^{-1} homogenous suspension of GO was prepared by dispersing 10 mg of GO in 20 mL of distilled water followed by ultrasonic agitation. Subsequently, 10 mL of GO (0.5 mg mL^{-1}) suspension was added to 10 mL of AuNR dispersion with ultrasonic agitation for 10 min followed by vigorous stirring for 2 h at room temperature. GO-AuNR nanocomposite was thus obtained.

Probe sequences, complementary and non-complementary target DNA

A 24-mer pork DNA probe sequence was selected from the cytochrome b (cytb) gene, verified by Hossain *et al.* (2017) to discriminate among cattle, buffalo and porcine materials in food by real-time PCR.[4] Furthermore, the selected DNA probe sequence was verified *in silico* by multiple alignments with the cytb gene of pork species in the presence of 27 other potential non-target species using MEGA5 software (http://www.megasoftware.net/). The alignment results showed 100% matching only with the pork cytb gene and 12.5–50% (3–12 nucleotides) mismatching with other non-target species (Table S1†). Moreover, the selected DNA probe sequence was divided into 12-mer lengths of two equal halves. The 5′ terminus of the probe sequence was chemically functionalized with ATTO-Rho6G, adjacent to the 6-carbon spacer arm (C6), followed by a terminal 5′ thiol modifier (S-S) (described in detail in the ESI†). Another part of the probe sequence was functionalized with a 3-carbon spacer arm with 3′ thiol modifier (C3 S-S). The chemically modified oligo DNA was synthesized and purified by Biosynthesis, USA (http://www.biosyn.com/index.aspx) while all other oligonucleotide sequences were obtained from Integrated DNA Technologies, Singapore (https://sg.idtdna.com/pages). All the oligo sequences used in this study are listed in Table S2 (ESI).† The lyophilized chemically modified oligonucleotide was dissolved in nuclease free water for reconstitution and kept as stock solution (100 μM) at −40 °C. The rest of the probe sequence and all other oligo sequences were reconstituted as per manufacturer instructions using TE buffer (pH 7.4) and kept as stock solutions (100 μM) at −40 °C.

Preparation of signal probe conjugated AuNPs

Thiol-modified chemically functionalized SP DNA (1 μM, 100 μL) was incubated with freshly prepared TCEP (10 mM, 10 μL) for at least 1 h at room temperature to reduce the disulfide bonds. Before functionalization, the as-prepared AuNPs (400 μL) were centrifuged at 8000 rpm for 30 min and the obtained AuNP pellet was re-dispersed in UPW to a final volume of 200 μL. The AuNPs were then functionalized with thiol-active single stranded (ss) SP DNA as per the protocol described in our previous study with minor modifications.[24] In detail, the TCEP-treated ATTO-Rho6G-intercalated SP DNA was mixed with AuNPs and incubated at room temperature for 16–20 h. The mixture was then treated with Tween 20 solution (0.1% Tween 20 in 10 mM PBS, pH 7.4) and incubated at room temperature for 30 min. This was followed by the salt aging of the suspension by the stepwise addition of NaCl (1 M) at intervals of 1 h or more to reach a concentration of 100 mM NaCl. During the salt aging process, a certain quantity of DNA is attached to AuNPs after each addition of NaCl and stabilizes the DNA functionalized AuNPs (AuNP-SP) for the next addition. Moreover, the conformation of the DNA probe on AuNPs changes from a horizontal array to vertical and keeps the nucleotide bases accessible for the subsequent hybridization process.[33] The AuNP-SP were allowed to age for another 40 h at room temperature under the same conditions. The main outcome of the prolonged salt-aging process is the decrease of repulsion between the DNAs to achieve an ultrahigh DNA density on the AuNPs.[34] Finally, the salt-aged AuNP-SP solution was centrifuged at 8000 rpm for 30 min, followed by discarding the supernatant to remove unbound DNA. The obtained AuNP-SP was resuspended in UPW and the washing procedure was repeated twice to keep the solution free from unbound DNA as much as possible.

Preparation of capture probe conjugated GO-AuNR

GO-AuNR were functionalized with the CP DNA as detailed in the literature with minor modifications.[35] The thiolated CP DNA was treated with TCEP as per the above mentioned procedure, mixed with GO-AuNR in water containing 0.01% sodium dodecyl sulfate and incubated overnight. This was followed by the addition of 10× TBE into the suspension to achieve a final buffer concentration of 1× TBE. After 4–5 h incubation, 1 M NaCl solution was added gradually to reach a final NaCl concentration of at least 100 mM by 24 h. The suspension was kept standing overnight at room temperature. The GO-AuNR-capture DNA probe (GO-AuNR-CP) composite was then washed with 1× TBE buffer by repeated centrifugation at 8000 rpm for 30 min to remove the excess unbound DNA and finally suspended in 0.1 mM PBS (pH 7.4).

Fabrication of the sandwich biosensor and acquisition of SERS spectra

The corresponding target DNA sequences (100 μL) were added to the AuNP-SP (200 μL) suspension and incubated overnight

at room temperature to facilitate the hybridization between the SP and target DNA. The suspension was washed with UPW by repeated centrifugation at 8000 rpm for 30 min to remove the unhybridized target DNA and the obtained partially hybridized composites (AuNP-SP-Target) were finally dispersed in 0.1 mM PBS (pH 7.4). Equal volumes of GO-AuNR-CP and AuNP-SP-Target were mixed together and incubated overnight at room temperature. During the incubation period, CP sequences hybridized with the unbound part of the target DNA attached to AuNPs-SP and formed the sandwich structure (GO-AuNR-CP-Target-SP-AuNP). Upon formation of the hybridized composite, purification was carried out by centrifugation at a very low speed (1000 rpm for 4 min) to separate the unbound AuNP-SP-Target or GO-AuNR-CP present in the supernatant. Afterward, the dual platform coupled sandwich biosensor composite was dispersed in 0.1 mM PBS (pH 7.4). Meanwhile, a silicon wafer was washed with ethanol, acetone and finally UPW before drying. The obtained final product (GO-AuNR-CP-Target-SP-AuNP, 30 μL) was dropped onto the silicon wafer and dried in vacuum atmosphere at ambient conditions for the SERS experiment. The SERS spectra were recorded using a Renishaw Invia confocal Raman microscope with a 20× objective lens and 532 nm laser as the light source. All obtained SERS data were analyzed using the Origin 2017 software.

Results and discussion

Characterization of GO, AuNPs, AuNRs and GO-AuNR

The synthesized GO, AuNPs, AuNR and GO-AuNR were characterized by UV-Vis spectroscopy, XRD, Raman spectroscopy and HR-TEM. The crystalline nature of the synthesized AuNPs was confirmed by XRD analysis and the obtained XRD patterns revealed five diffraction peaks at 2θ = 38.25°, 44.40°, 64.68°, 77.69° and 81.84° (Fig. S2†), which are assigned to the (111), (200), (220), (311) and (222) lattice planes of FCC AuNPs (JCPDS no. 04-0784). The high intensity diffraction peak at 2θ = 38.18° corresponds to the (111) plane, indicating its predominant orientation. The as-prepared burgundy red colored AuNPs showed an absorption band at 519 nm in the UV-Vis spectrum (Fig. 1a) and were confirmed by the AFM (Fig. S3a and b†) and HR-TEM images where AuNPs were observed to be spherical in shape with sizes ranging from 12 to 14 nm in diameter (Fig. 2a).

The oxidative synthesis of GO from graphite flakes was confirmed by XRD analysis with a diffraction peak at 2θ = 10.24° (Fig. S2†).[36] The UV-Vis spectrum of ultrasonicated and well dispersed GO suspension in water showed a characteristic absorption peak at 233 nm (Fig. 1b), which was confirmed by the HR-TEM (Fig. 2b) and AFM topography images (Fig. S3c and d†) of GO. In the HRTEM image, GO was characterized by its typical crumpled flake structure. UV–Vis–NIR absorption spectra of the as-prepared AuNRs showed two absorption peaks at 522 and 827 nm (Fig. 1b), which are due to the transverse and longitudinal plasmon resonance absorptions, respectively.[32,37] The TEM image of AuNR displayed the high quality of AuNRs with uniform shape and size, average diameter of 12 ± 2 nm and average length of 55 ± 7 nm (Fig. 2c). UV-Vis and TEM studies of AuNRs therefore correlate and correspond with previous studies.[31,38]

XRD spectra of GO-AuNR hybrid showed peaks at 2θ = 11.8°, 21.36°, 38.30°, 44.36°, 64.56° and 77.60° (Fig. S2†) where the peak at 2θ = 11.8° is attributed to the corresponding GO peak and the peak at 2θ = 21.36° indicated partial reduction of GO, which might be due to the ultrasonication and prolonged vigorous stirring. However, the other diffraction peaks at 38.30° (111), 44.36° (200), 64.56° (220) and 77.60° (311) are attributed to the presence of AuNRs over GO.[39] Moreover, the UV-Vis spectrum of the GO-AuNR hybrid showed three peaks at 245, 511 and 821 nm, where the peak at 245 nm represents the characteristic but shifted absorption peak of GO and the peaks at 511 and 821 nm respectively represent the transverse and longitudinal plasmon bands of AuNR, which

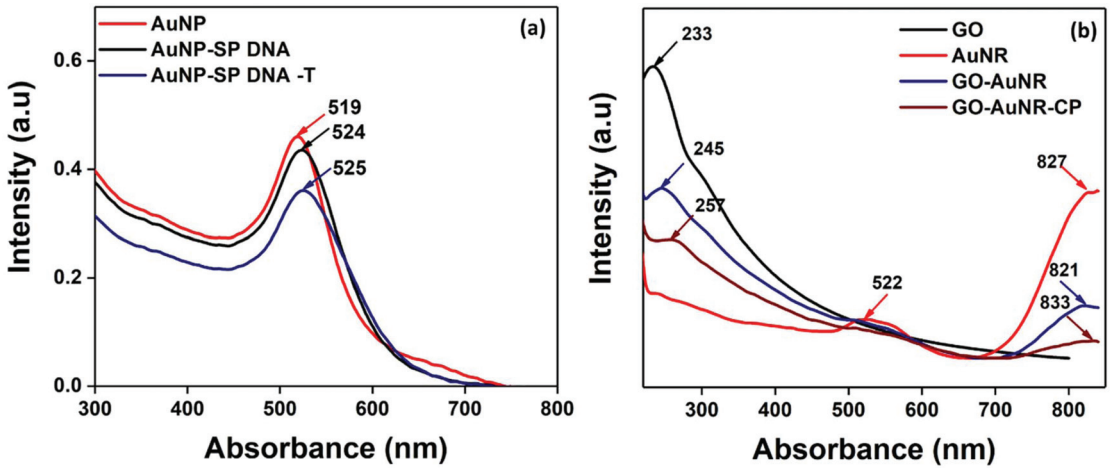

Fig. 1 UV-Vis absorption spectra of (a) AuNPs, AuNPs functionalized with the thiolated signal probe, AuNP-linked SP with partially hybridized target DNA, (b) GO, AuNR, GO-AuNR, and GO-AuNR functionalized with the capture probe DNA.

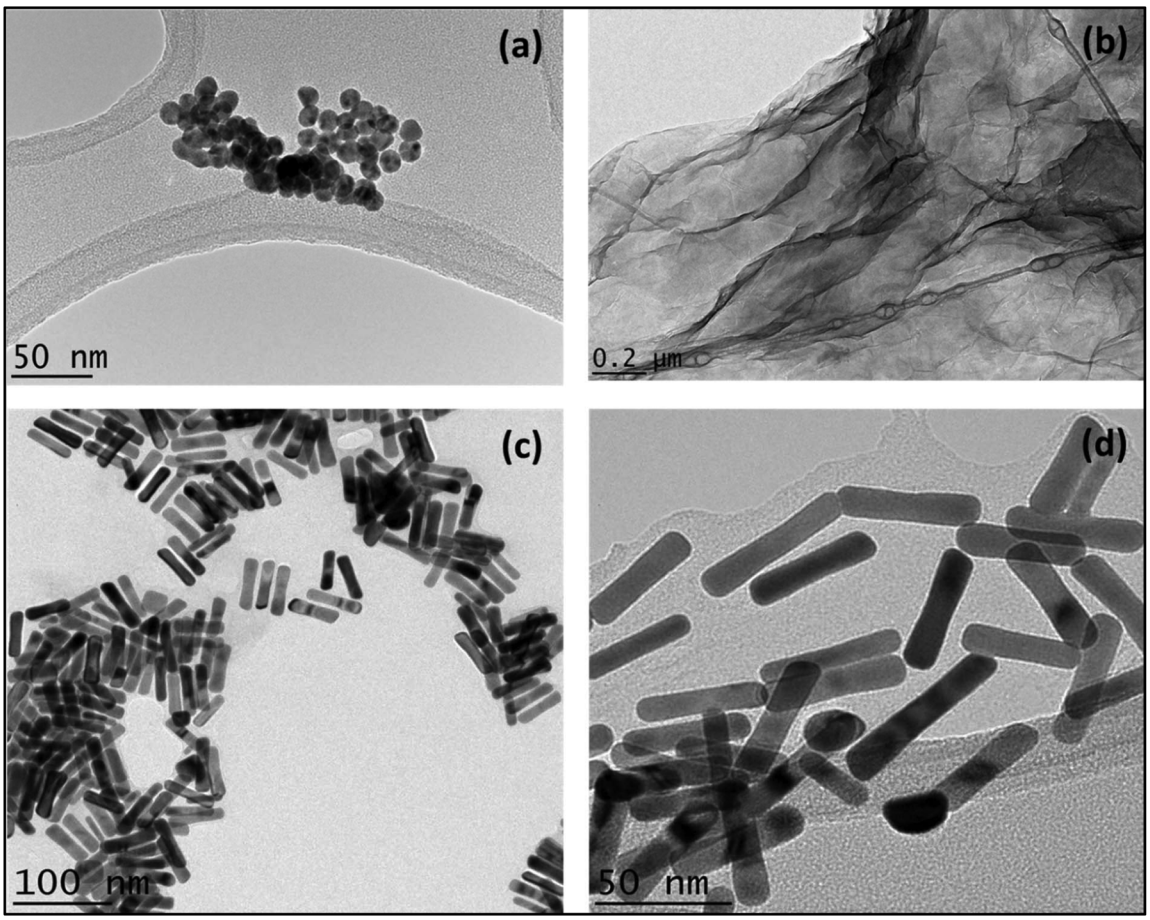

Fig. 2 HR-TEM images of (a) AuNPs, (b) GO, (c) AuNR, and (d) GO-AuNR samples prepared on lacy carbon coated copper grid.

are shifted a bit in comparison to pure AuNRs (Fig. 1b). This peak shifting is from the plasmon coupling between AuNRs and GO, in compliance with the HR-TEM and AFM studies. It was observed in the HR-TEM image that the near-transparent GO is perfectly decorated by a large number of well dispersed AuNRs (Fig. 2d), thereby confirming the strong interaction between GO and AuNRs, which was further verified by the well-scattered AuNRs over GO sheets in the AFM study (Fig. S3e and f†). Therefore, the XRD, TEM and AFM characterization studies of the *ex situ* synthesized GO-AuNR confirm the homogenous distribution of the uniformly size-ranged AuNR over GO sheets *via* strong electrostatic attraction.[32,39]

Attachment of the DNA probe sequences onto sensor platforms

Attachment of the 12-mer long ss SP DNA on the AuNP surface *via* thiol–gold linkage is confirmed by the peak shift from 519 nm to 524 nm in the UV-Vis spectrum (Fig. 1a). The 5 nm red shift is due to the increase of the AuNP particle size from the formation of a single layer of probe sequences and therefore confirms the successful attachment of DNA onto the AuNP surface. In addition, there was no significant color change in the AuNPs solution, also confirming the absence of AuNP aggregation during the salt aging steps.[40] The hybridization of the corresponding target DNA with the SP sequences linked to AuNPs showed a further slight shift (1 nm) in the UV-Vis spectrum. Similarly, the UV-Vis absorption spectrum of the ss CP DNA covalently linked to GO-AuNR hybrid exhibited a red shift of the characteristic AuNR peak from 821 to 833 nm (Fig. 1b), thus confirming the successful attachment of the thiolated DNA to the AuNRs of the hybrid composite.

Principle and justification of the SERS DNA biosensing technique

In the biosensor fabrication, the SP DNA with the unique incorporation of ATTO Rho6G immediately after the C6 spacer was immobilized onto the AuNPs *via* the Au–S linkage between AuNPs and the terminal thiol molecule of the SP sequences (Scheme 1a).[41] Here, the C6 spacer assists the SP sequences to stand in an upright position, making SP accessible for hybridization and holding the Raman tag a few nanometers from the AuNPs surface, which ensures the SERS effect *via* both electromagnetic and charge transfer mechanisms. On the other hand, CP sequences were attached on the GO-AuNR hybrid *via* covalent bonding between the terminal thiol molecule of the probe sequences and the AuNR of the GO-AuNR hybrid compo-

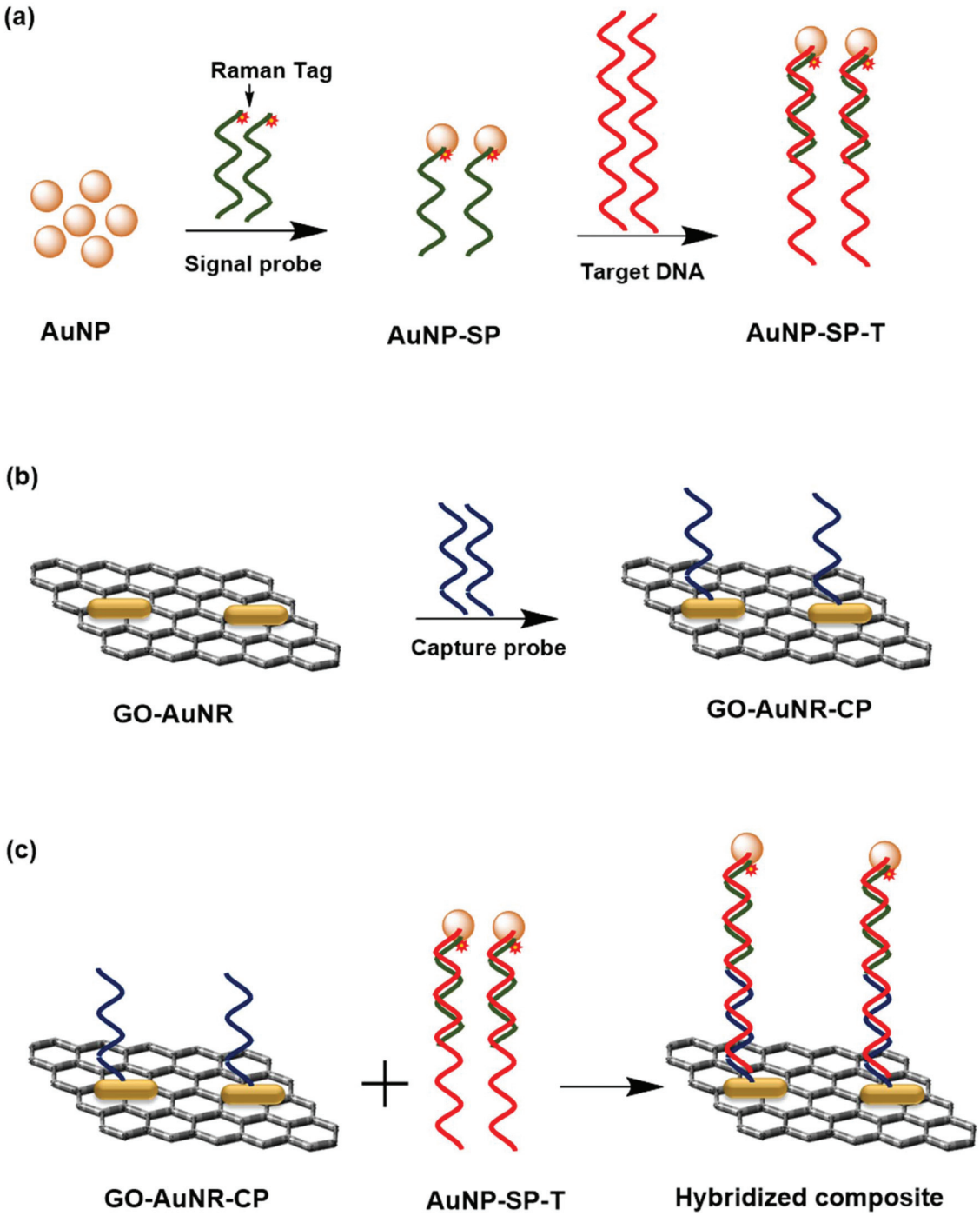

Scheme 1 Schematic representation of the SERS DNA biosensing strategy using GO-AuNR and AuNP platforms.

site (Scheme 1b). To immobilize the CP sequences, the C3 spacer molecule next to the disulfide bond keeps the DNA strands upright, by minimizing the steric effects between the nucleotide bases and surfaces of AuNRs,[41] and accessible to the nucleotide bases for hybridization. Therefore, the partial hybridization of the target sequences with the SP linked to AuNPs, followed by the formation of the sandwich complex *via* binary covalent linking between the CP with the remainder of the free target sequence joins the two platforms together (Scheme 1c), thereby enhancing the SERS signal due to the multicomponent aggregate hot spots-induced electromagnetic and Raman-tag-contributed chemical enhancement.[42,43]

The successful attachment of SP on the AuNPs was confirmed by the distinct fingerprint SERS spectrum of ATTO Rho6G, attributed to the peaks at 774, 1126, 1184, 1359, 1507, 1569 and 1647 cm^{-1}, which corresponds to the Raman spec-

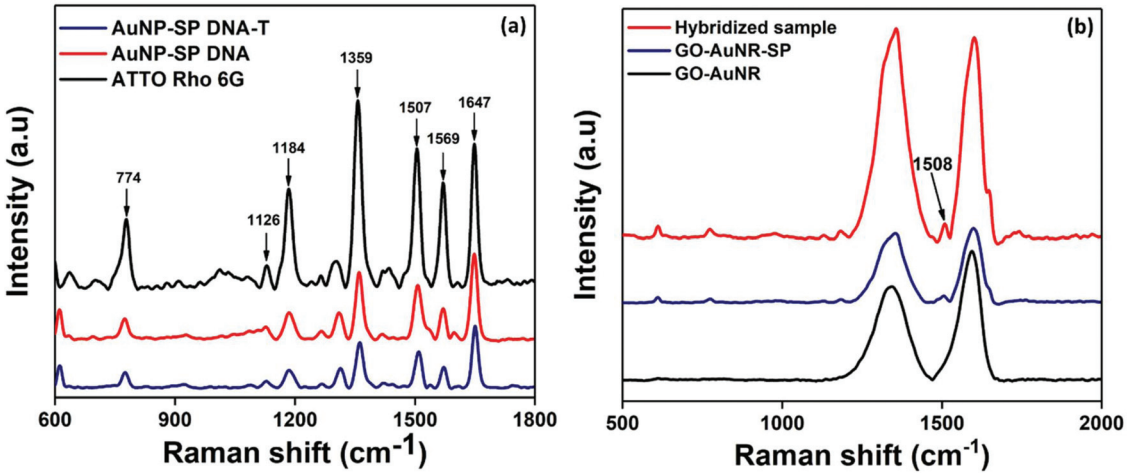

Fig. 3 Raman spectra of (a) pure ATTO Rho6G, AuNPs first functionalized with SP DNA intercalated with ATTO Rho6G and subsequently partially hybridized with the corresponding target DNA, (b) GO-AuNR, GO-AuNR functionalized with SP DNA and the hybridized composite GO-AuNR-CP-Target-SP-AuNP.

trum of pure ATTO Rho6G (Fig. 3a). However, the Raman intensity of SP-functionalized AuNPs is lower than that of the pure ATTO Rho6G dye alone, which is definitely due to the lower number of ATTO Rho6G molecules, as each SP is integrated with only one Raman tag. Moreover, the partial hybridization of the SP sequences with the corresponding target sequences has no impact on the spectral fingerprint; rather, a decreased intensity was observed due to the loss of SP sequences by repetitive washing (Fig. 3a). The Raman spectrum of the SERS-active CP-linked GO-AuNR substrate exhibits only the characteristic D and G bands of GO. However, the SERS spectrum of GO-AuNR immobilized SP sequences was characterized by the D and G bands as well as ATTO Rho6G fingerprint peaks, mainly at 1508 cm^{-1}, along with a few other peaks at 610, 774, 1184 and 1647 cm^{-1} (Fig. 3b). This unique spectrum therefore confirms the successful immobilization strategy of probe sequences onto GO-AuNR platform as well as the pattern and position of the ATTO Rho6G fingerprint peaks. The SERS spectrum of the hybridized composite also revealed an identical but more intense spectrum to the GO-AuNR-SP composite, including the D band at 1356 cm^{-1}, G band at 1600 cm^{-1} and the dominant peak representing ATTO Rho6G at 1508 cm^{-1}, in addition to the presence of peaks at 610, 774, 1184 and 1647 cm^{-1} (Fig. 3b).[44] This confirms the hybridization of the DNA probes with the corresponding target DNA and the consequent coupling of the two platforms. Hence, based on this biosensing strategy, the intensity of the ATTO Rho6G, which represents the fingerprint peaks of the hybridized composites, can be correlated to the amount of corresponding target DNA. Therefore, the peak at 1508 cm^{-1} was selected as the standard peak for the qualitative and quantitative detection of the target pork DNA throughout the study.

The linking of the two platforms was also confirmed by the HR-TEM images of the hybridized products (Fig. 4a–d), in which the AuNPs were attached to the AuNRs of the GO-AuNR composites. This indicates successful hybridization between the complementary target sequences with the two strands of CP and SP sequences. However, a few AuNPs were also found on the GO sheets, indicating non-specific adsorption of AuNPs over the GO-AuNRs. This suggests a failure of hybridization due to the absence of DNA probe sequences or the absence of complementary target sequences to be hybridized.[45]

Performance of the dual platform based SERS DNA biosensor

Quantitative detection of the target DNA was accomplished by determining the intensity of the representative SERS peak at 1508 cm^{-1} for the ATTO Rho6G intercalated in the SP DNA. The quantitative evaluation was performed by varying the concentration of target DNA from 10 aM to 1 μM and showed a steady upward trend of the SERS signal intensity at 1508 cm^{-1} (Fig. 5a and b). However, no ATTO Rho6G fingerprint peak at 1508 cm^{-1} was distinguishable for the hybridized composite at a target DNA concentration of 10 aM, while the peak of the 100 aM concentration of target DNA was still well distinguished and detectable; therefore, 10 aM is considered the LOD. Moreover, the peak intensity showed a linear response with respect to the target DNA concentration from 100 aM to 1 μM with a correlation coefficient value (R^2) of 0.9828. The error bars were calculated by three repeated measurements of each concentration of target DNA (Fig. 5c). Compared to other works on DNA detection, this dual platform based SERS biosensor with a very short-length DNA probe provides higher sensitivity for detecting minute amounts of DNA in the sample. The excellent performance of this fabricated biosensor relies on the use of two different SERS-active platforms and the Raman dye-intercalated short-length DNA probe in which the ATTO Rho6G was spontaneously positioned within a few nanometers of the AuNPs surface due to the unique design of the DNA probe. In addition, the GO-AuNRs nanocomposite, as the sensor platform, has great influence on SERS signal enhance-

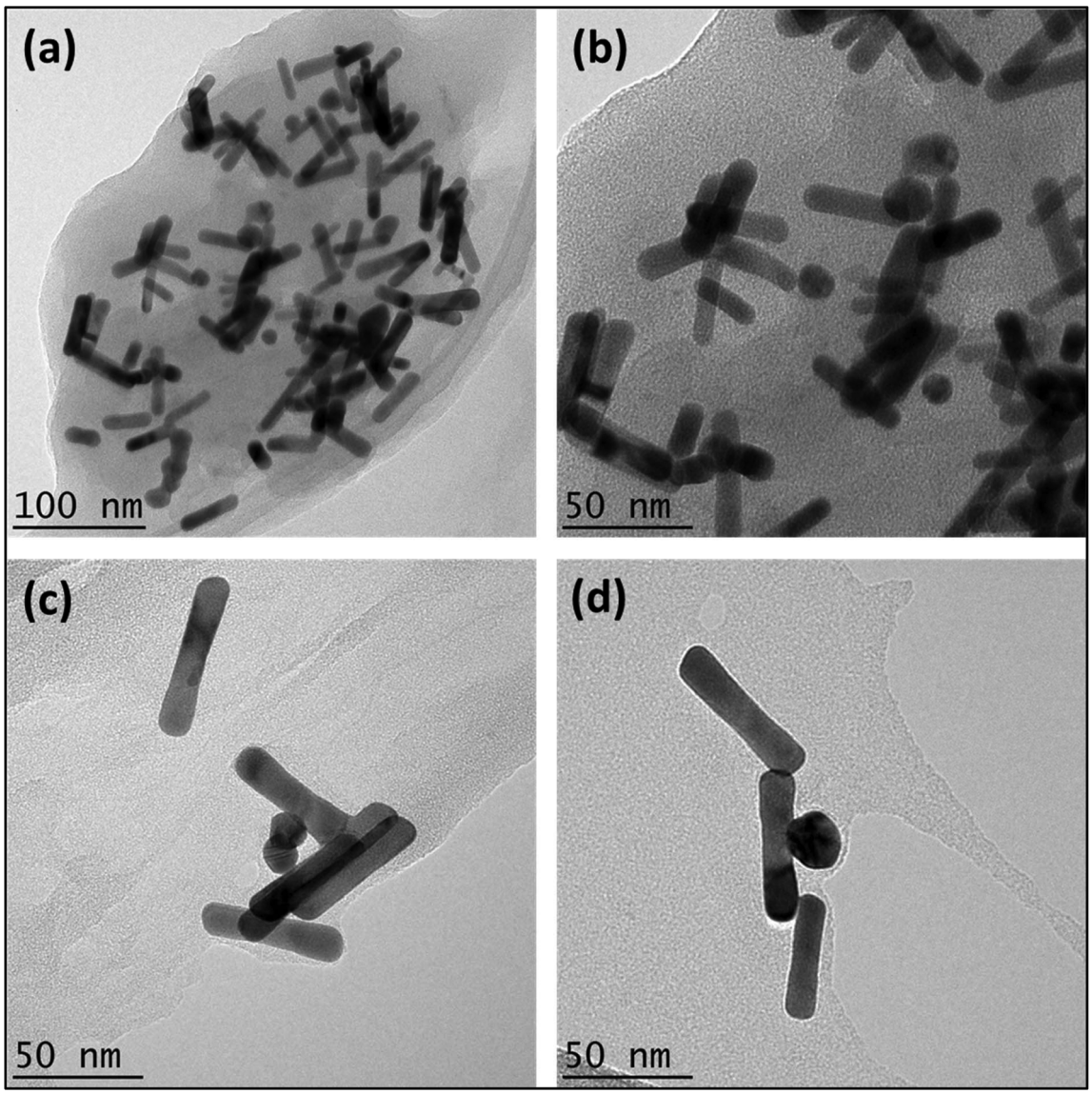

Fig. 4 HR-TEM images of the hybridized composites (GO-AuNR-CP-Target-SP-AuNP) at 100 nm (a) and 50 nm (b–d) magnifications. The hybridized composites were formed *via* probe–target hybridization mediated coupling of AuNPs onto GO-AuNR. In the images, the AuNPs are mostly found attached to the AuNRs of GO-AuNR hybrid, indicating successful hybridization.

ment owing to the strong light scattering and local field enhancement properties of AuNRs induced by the anisotropic splitting of the SPR into transverse SPR and longitudinal SPR, as well as the synergistic effect of GO and AuNR components.[30,38] Moreover, the coupling of the two platforms *via* hybridization between the target DNA with the signal and capture probes brought together the GO-AuNR and AuNP, consequently generating hot spots at the nanoparticle junctions that led to an increased SERS signal by electromagnetic enhancement.[46] Furthermore, the two platforms were attached *via* probe–target sequence linking; hence, the ATTO Rho6G integrated into the SP sequences was aligned in the interstices of the GO-AuNR and AuNPs, where the hot spots actually originate. The Raman tag also directly contributes to the SERS signal enhancement by the charge transfer mechanism between the AuNPs and Raman dye.[47,48] The dual platforms and the Raman tag functionalized SP have an overall influence on the SERS intensity through the combined effects of electromagnetic and chemical enhancement mechanisms, hence increasing the sensitivity of detection.

This fabricated biosensor based on short-length split DNA markers with direct incorporation of the Raman tag to the DNA sequences is a novel approach that exerts no hindrance on hybridization, but rather enhances the SERS signal and is therefore advantageous for the detection of DNA. It also exhibited better performance compared to the biosensor fabricated by our group using the dual SERS-active platforms, co-adsorption of Raman tag along with the probe sequence on AuNPs

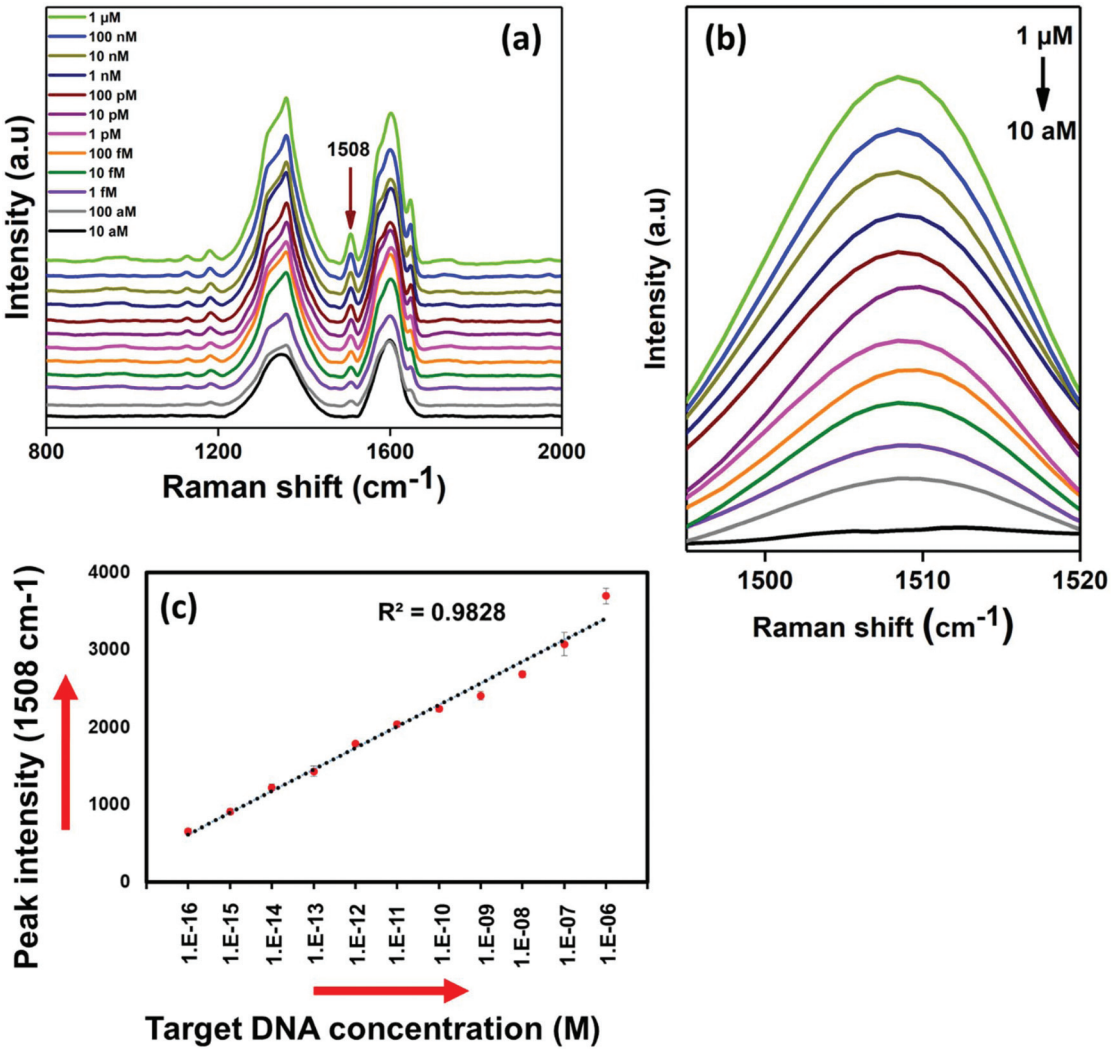

Fig. 5 (a) The stacked SERS spectra of hybridized composites obtained from the target DNA of pork species from 1 μM to 10 aM. (b) The spectra of the hybridized composites (1 μM to 10 aM) cropped to 1490 to 1520 cm^{-1} to magnify and distinguish the intensity of the peak at 1508 cm^{-1}. (c) The linear curve of SERS intensity at 1508 cm^{-1} *vs.* target DNA concentration. Error bars were calculated from three repeated Raman scan results for each target DNA concentration.

and following the same hybridization principle for detecting MBT.[45] Moreover, this biosensor is efficient compared to the biosensors comprised of a single platform and using reporter DNA with a Raman tag labelled at a terminal end,[49] either SERS non-active[44,50] or SERS active dual platforms using the sandwich assay procedure.[51,52] Therefore, to minimize the shortcomings of the previously reported SERS DNA biosensors as well as to adopt a straightforward and convenient technique, herein, we have employed dual SERS-active platforms with Raman tag intercalated SP DNA. Moreover, the fabricated SERS biosensor showed greater efficiency toward the detection of pork compared to other techniques such as PCR,[16,53] colorimetry,[54] enzyme immunoassay[13] and electrochemical detection techniques.[21] To the best of our knowledge, this is the first reported SERS technique for the detection of pork residues. Hence, this SERS DNA detection strategy could be considered efficient for the definite identification of pork residues as a quality control or screening procedure in the food chain or in industrial applications.

Selectivity, specificity and reproducibility study of the biosensor

The selectivity of the biosensor platform was investigated by assessing the hybridization capability of the biosensor with non-target DNA as interference factors. Because of its complementary nature, only the corresponding target DNA of pork hybridizes with the probe sequences and forms duplex structures, as characterized by the appearance of the D and G bands of GO with an obvious distinct peak at 1508 cm^{-1} attributed to the ATTO Rho6G (Fig. 6a). This intense SERS spectrum is due to the generation of hot spots at the interstices between GO-AuNR and AuNPs,[55] indicating a positive result. As

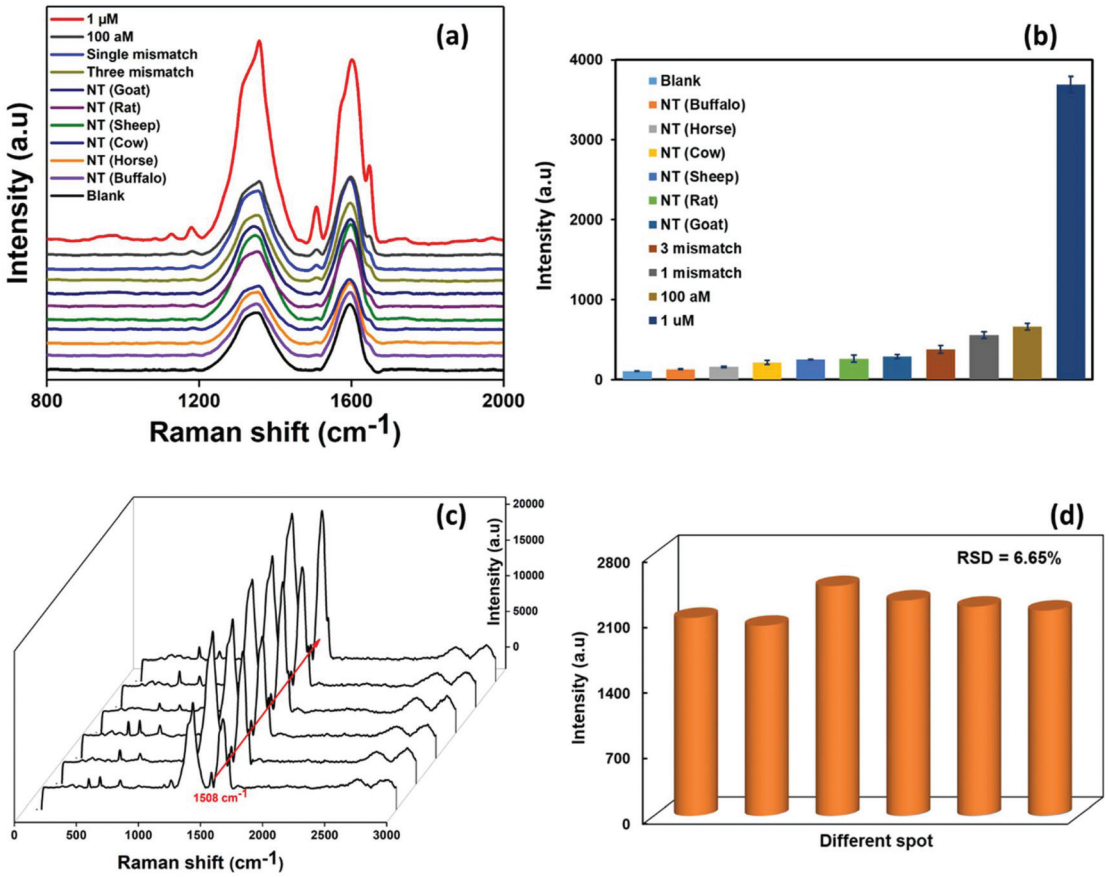

Fig. 6 (a) SERS spectra for the selectivity study of the fabricated biosensors using different DNA sequences: complementary (1 μM), LOD concentration (100 aM), 1 μM concentration of blank sample, single mismatch, triple mismatches and interference samples (non-target sequences of goat, rat, sheep, cow, horse and buffalo) and (b) the corresponding intensity of the SERS fingerprint signals at peak position 1508 cm^{-1}. Standard error bars were the outcome of three consecutive measurements obtained at each DNA concentration. (c) SERS spectra of the hybridized composite (100 pM target DNA) from six different spots and (d) the RSD of the SERS peak intensity at 1508 cm^{-1} for 6 different spots.

depicted in Fig. 6a and b, the blank sample (negative control) and interference samples (non-target DNA sequences of goat, rat, sheep, cow, horse and buffalo) at a concentration of 1 μM produced low Raman intensity for the peak at 1508 cm^{-1}, the signatory peak of hybridization. Therefore, the peak intensity at 1508 cm^{-1} for the blank sample was considered the baseline signal for the ATTO Rho6G and the obtained spectrum is denoted as the true negative. However, the small ATTO Rho6G signal from the blank as well as the non-target treated hybridized composite might be due to a non-specific interaction between the fabricated GO-AuNRs-CP and AuNPs-SP-Target composites.[45] Therefore, the results of the interference study showed that the SERS intensity of the ATTO Rho6G signal at 1508 cm^{-1} was much stronger in the presence of the target sequence compared to the other non-target DNA of variable length and nucleotide mismatches, indicating the excellent selectivity of the biosensor for the detection of pork DNA.

Furthermore, the biosensor was tested to differentiate target DNA with a single nucleotide base mismatch and three-base mismatches. The SERS intensity of the ATTO Rho6G signal at 1508 cm^{-1} from the hybridized composite formed by the single base-mismatch was more intense than the three-base mismatches (Fig. 6b). Both these SERS spectra were obviously less intense compared to the complementary target sequences, but more intense compared to the other interference non-target DNA (Fig. 6b). This is attributed to the hybridization between the single-base mismatch target sequences with the SP followed by the CP sequences. However, the chances of hybridization are lowered by the mismatch of bases. The plots in Fig. 6a and b indicate a lower occurrence of hybridization, so the lower SERS intensity is due to the larger number of nucleotide mismatches in the sequence. We believe the excellent specificity of this fabricated biosensor is due to the selection of a short-length DNA probe, which was further split to produce two very short segments of DNA probe sequences that can easily recognize complementary nucleotide bases in the target sequences.[24]

Validation of the hybridization procedure, preparation of samples for Raman experiments, and the repeatability of the SERS-based DNA biosensors were justified by the SERS spectra from six different randomly chosen points of a slide prepared with the hybridized composite and 100 pM target. All the SERS

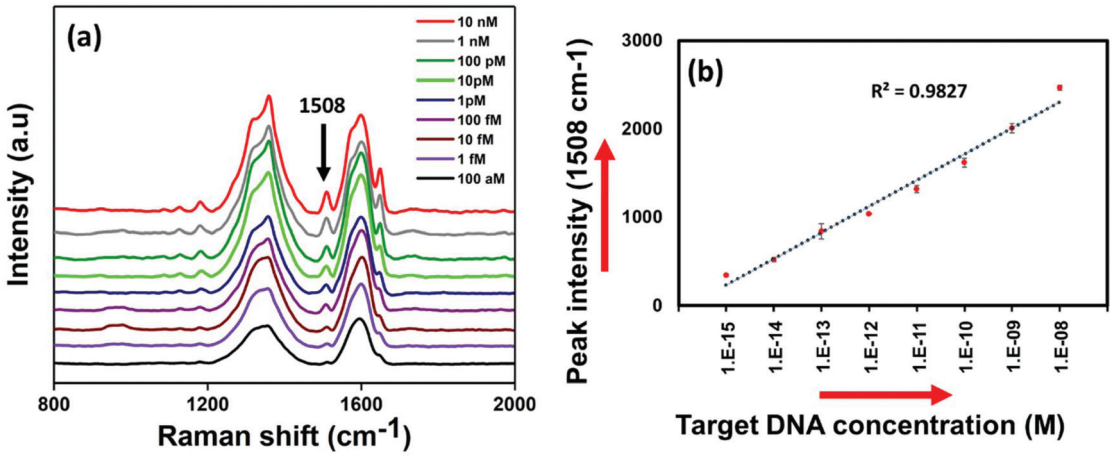

Fig. 7 (a) SERS spectra for the hybridized composites with target DNA (100 aM to 10 nM) from real pork samples. (b) The linear curve of SERS intensity at 1508 cm^{-1} *vs.* target DNA concentration for the real sample.

shapes are generally alike (Fig. 6c) and the relative standard deviation (RSD) value of the corresponding SERS intensity of the representative peak (1508 cm^{-1}) is only 6.65% (Fig. 6d), which indicates that the hybridization occurred uniformly throughout the reaction system and the method is reproducible.

Application of the SERS DNA biosensor for real samples

To validate the feasibility and efficiency of the fabricated SERS biosensor, DNA extracted from the pork sample (described in ESI†) was used. The extracted pork DNA was further diluted to attain the LOD concentration that was established for the synthetic target DNA. The serially diluted DNA solution was then heat-treated in a water bath at 95 °C for 15 min, followed by rapid cooling in an ice bath for further 15 min and finally ultrasonication of the heat-treated denatured ssDNA solution for 20 min to obtain small-fragment ssDNA.[56,57] The fabricated sensor showed extraordinary sensitivity for the detection of the corresponding target DNA from real samples. The SERS peaks at 1508 cm^{-1} for the DNA concentrations from 10 nM to 1 fM were well distinguished. The LOD was established as 1 fM (Fig. 7a), which is 10 times lower than the obtained results (100 aM) for the synthesized synthetic target DNA. The curve obtained from the peak intensity at 1508 cm^{-1} *vs.* target DNA concentration also showed an excellent linear relationship with an R^2 value of 0.9827 (Fig. 7b). The lower LOD value may be due to the variable length of the corresponding target DNA and the presence of some inhibitory components from the extraction procedure. Therefore, it can be concluded that the efficiency of the coupling of two platforms using real DNA sample mediated hybridization is well-justified for practical applications.

Conclusion

In this work, the 24-mer length DNA probe sequence used for the detection of pork DNA was split into two parts. The 5′ terminal was chemically functionalized using a novel design with ATTO Rho6G adjacent to the C6 spacer arm with a terminal thiol modifier and immobilized onto AuNPs surface. The 3′ end of the split-probe DNA was functionalized with C3-S-S and immobilized onto SERS-active GO-AuNRs. The introduction of complementary target sequences coupled the two platforms *via* the target–probe sequence hybridization and consequently produced an identical, distinguishable and enhanced SERS signal. The greater SERS intensity is due to the combined effect of electromagnetic and chemical enhancements at the hot spot region originating at the junction of GO-AuNRs and AuNPs. Therefore, by the combination of the two different platforms and a very short-length Raman tagged DNA probe sequence, the fabricated biosensor showed an LOD as low as 100 aM and differentiated the DNA sequences of closely related non-target species (goat, rat, sheep, cow, horse and buffalo) and a single-base mismatch in the complementary target sequences. Moreover, the biosensor was validated for real sample analysis. The biosensor thus exhibited excellent selectivity, sensitivity and efficiency for the qualitative and quantitative detection of pig DNA, which is a potential application in industries and regulatory agencies. Thus, it is believed that, as a whole, this approach could be considered a model and adopted for forensic applications, detection of various pathogenic microorganisms and even cancer detection using very short DNA markers. Finally, we strongly believe that different SERS-active sensor platforms using this facile fabrication procedure and a species-specific Raman tag integrated into short-length oligo probe sequences could lead to the fabrication of multiplex biosensors for the detection of a panel of biomarkers, which is in high demand.

Conflicts of interest

The authors declare no conflict of interest.

Acknowledgements

This research work was financially supported by the Grand Challenge Project (GC001B-14SBS), and Postgraduate Research Grant (PPP) (PG190-2015B) of the University of Malaya, Malaysia and Grant number, FP039-2016 of the Ministry of Higher Education, Malaysia. The authors would like to acknowledge Dr M. A. Motalib Hossain, University of Malaya for providing the pork meat samples and the lab facility for DNA handling and storage.

References

1 P. O'mahony, *QJM*, 2013, **106**, 595–597.
2 T. Jaques, *Corp. Commun. Int. J.*, 2015, **20**, 468–482.
3 E. Whitworth, A. Druckman and A. Woodward, *Br. Food J.*, 2017, **119**, 131–142.
4 M. M. Hossain, M. E. Ali, S. Sultana, S. Q. Bonny, M. A. Kader and M. A. Rahman, *J. Agric. Food Chem.*, 2017, **65**, 3975–3985.
5 J. Premanandh, *Food Control*, 2013, **34**, 568–569.
6 A. M. Griffiths, C. G. Sotelo, R. Mendes, R. I. Pérez-Martín, U. Schröder, M. Shorten, H. A. Silva, V. Verrez-Bagnis and S. Mariani, *Food Control*, 2014, **45**, 95–100.
7 R. Liu, X. Wang, X. Wang, Y. Shi, C. Shi, W. Wang and C. Ma, *Food Control*, 2019, **98**, 297–302.
8 J. Fischer, *Geoforum*, 2016, **69**, 67–70.
9 V. Skouridou, H. Tomaso, J. Rau, A. S. Bashammakh, M. S. El-Shahawi, A. O. Alyoubi and C. K. O'Sullivan, *Food Chem.*, 2019, **287**, 354–362.
10 N. Giaretta, A. M. A. Di Giuseppe, M. Lippert, A. Parente and A. Di Maro, *Food Chem.*, 2013, **141**, 1814–1820.
11 M. Montowska and E. Pospiech, *Food Chem.*, 2013, **136**, 1461–1469.
12 Y. Kumar and S. C. Karne, *Trends Food Sci. Technol.*, 2017, **62**, 59–67.
13 J. Mandli, I. E. Fatimi, N. Seddaoui and A. Amine, *Food Chem.*, 2018, **255**, 380–389.
14 B. Kuswandi, A. A. Gani and M. Ahmad, *Food Biosci.*, 2017, **19**, 1–6.
15 M. M. Hossain, M. E. Ali, S. B. Abd Hamid, S. Mustafa, M. N. Mohd Desa and I. Zaidul, *J. Agric. Food Chem.*, 2016, **64**, 6343–6354.
16 T. S. Kang and T. Tanaka, *Food Chem.*, 2018, **269**, 549–558.
17 J.-H. Lee, M.-R. Kim, C.-H. Jo, Y.-K. Jung, K. Kwon and T. S. Kang, *Food Chem.*, 2016, **211**, 253–259.
18 M. E. Ali, U. Hashim, S. Mustafa and Y. B. C. Man, *Food Anal. Methods*, 2012, **5**, 613–623.
19 M. Ali, U. Hashim, S. Mustafa, Y. Man and K. N. Islam, *J. Nanomater.*, 2012, **2012**, 1.
20 R. Hu, T. Liu, X.-B. Zhang, S.-Y. Huan, C. Wu, T. Fu and W. Tan, *Anal. Chem.*, 2014, **86**, 5009–5016.
21 S. Roy, I. A. Rahman, J. H. Santos and M. U. Ahmed, *Food Control*, 2016, **61**, 70–78.
22 L.-J. Xu, Z.-C. Lei, J. Li, C. Zong, C. J. Yang and B. Ren, *J. Am. Chem. Soc.*, 2015, **137**, 5149–5154.
23 K. Kneipp, H. Kneipp and H. G. Bohr, in *Surface-Enhanced Raman Scattering*, Springer, 2006, pp. 261–277.
24 I. Khalil, W. A. Yehye, N. M. Julkapli, S. Rahmati, A. A. I. Sina, W. J. Basirun and M. R. Johan, *Biosens. Bioelectron.*, 2019, **131**, 214–223.
25 Y.-H. Sun, R.-M. Kong, D.-Q. Lu, X.-B. Zhang, H.-M. Meng, W. Tan, G.-L. Shen and R.-Q. Yu, *Chem. Commun.*, 2011, **47**, 3840–3842.
26 S. Zou and G. C. Schatz, in *Surface-Enhanced Raman Scattering*, Springer, 2006, pp. 67–85.
27 I. Khalil, N. M. Julkapli, W. A. Yehye, W. J. Basirun and S. K. Bhargava, *Materials*, 2016, **9**, 406.
28 E. Hao and G. C. Schatz, *J. Chem. Phys.*, 2004, **120**, 357–366.
29 X. Qian, X. Zhou and S. Nie, *J. Am. Chem. Soc.*, 2008, **130**, 14934–14935.
30 P. G. Vianna, D. Grasseschi, G. K. Costa, I. C. Carvalho, S. H. Domingues, J. Fontana and C. J. de Matos, *ACS Photonics*, 2016, **3**, 1027–1035.
31 L. Feng, Z. Xuan, J. Ma, J. Chen, D. Cui, C. Su, J. Guo and Y. Zhang, *J. Exp. Nanosci.*, 2015, **10**, 258–267.
32 X. Han, X. Fang, A. Shi, J. Wang and Y. Zhang, *Anal. Biochem.*, 2013, **443**, 117–123.
33 X. Zhang, T. Gouriye, K. Göeken, M. R. Servos, R. Gill and J. Liu, *J. Phys. Chem. C*, 2013, **117**, 15677–15684.
34 B. Liu and J. Liu, *Anal. Methods*, 2017, **9**, 2633–2643.
35 S. Pal, Z. Deng, H. Wang, S. Zou, Y. Liu and H. Yan, *J. Am. Chem. Soc.*, 2011, **133**, 17606–17609.
36 D. C. Marcano, D. V. Kosynkin, J. M. Berlin, A. Sinitskii, Z. Sun, A. Slesarev, L. B. Alemany, W. Lu and J. M. Tour, *ACS Nano*, 2010, **4**, 4806–4814.
37 J. Zhang, Y. Sun, B. Xu, H. Zhang, Y. Gao, H. Zhang and D. Song, *Biosens. Bioelectron.*, 2013, **45**, 230–236.
38 J. Guo, T. Ning, Y. Han, Y. Sheng, C. Li, X. Zhao, Z. Lu, B. Man, Y. Jiao and S. Jiang, *Appl. Surf. Sci.*, 2018, **433**, 45–50.
39 G. Tao and J. Wang, *Carbon*, 2018, **133**, 209–217.
40 J. Thavanathan, N. M. Huang and K. L. Thong, *Biosens. Bioelectron.*, 2014, **55**, 91–98.
41 J. Zhang, S. Song, L. Wang, D. Pan and C. Fan, *Nat. Protoc.*, 2007, **2**, 2888–2895.
42 R. C. Mucic, J. J. Storhoff, C. A. Mirkin and R. L. Letsinger, *J. Am. Chem. Soc.*, 1998, **120**, 12674–12675.
43 L. Sun, C. Yu and J. Irudayaraj, *Anal. Chem.*, 2007, **79**, 3981–3988.
44 J. Prinz, A. Matković, J. Pešić, R. Gajić and I. Bald, *Small*, 2016, **12**, 5458–5467.
45 I. Khalil, W. A. Yehye, N. M. Julkapli, S. Rahmati, A. A. I. Sina, W. J. Basirun and M. R. Johan, *Biosens. Bioelectron.*, 2019, **131**, 214–223.
46 T.-W. Lin, H.-Y. Wu, T.-T. Tasi, Y.-H. Lai and H.-H. Shen, *Phys. Chem. Chem. Phys.*, 2015, **17**, 18443–18448.
47 R. C. Maher, in *Raman Spectroscopy for Nanomaterials Characterization*, ed. C. S. S. R. Kumar, Springer Berlin Heidelberg, Berlin, Heidelberg, 2012, pp. 215–260.

48 D. Radziuk and H. Moehwald, *Phys. Chem. Chem. Phys.*, 2015, **17**, 21072–21093.
49 S. He, K.-K. Liu, S. Su, J. Yan, X. Mao, D. Wang, Y. He, L.-J. Li, S. Song and C. Fan, *Anal. Chem.*, 2012, **84**, 4622–4627.
50 Y. C. Cao, R. Jin and C. A. Mirkin, *Science*, 2002, **297**, 1536–1540.
51 H. Zhang, M. H. Harpster, H. J. Park, P. A. Johnson and W. C. Wilson, *Anal. Chem.*, 2010, **83**, 254–260.
52 T. Kang, S. M. Yoo, I. Yoon, S. Y. Lee and B. Kim, *Nano Lett.*, 2010, **10**, 1189–1193.
53 R. Xu, S. Wei, G. Zhou, J. Ren, Z. Liu, S. Tang, P. C. Cheung and X. Wu, *Meat Sci.*, 2018, **137**, 41–46.
54 S. Roy, N. F. Mohd-Naim, M. Safavieh and M. U. Ahmed, *ACS Sens.*, 2017, **2**, 1713–1720.
55 T. T. Chuong, A. Pallaoro, C. A. Chaves, Z. Li, J. Lee, M. Eisenstein, G. D. Stucky, M. Moskovits and H. T. Soh, *Proc. Natl. Acad. Sci. U. S. A.*, 2017, **114**, 9056–9061.
56 C. M. Pandey, G. Sumana and B. D. Malhotra, *Biomacromolecules*, 2011, **12**, 2925–2932.
57 I. Tiwari, M. Gupta, C. M. Pandey and V. Mishra, *Dalton Trans.*, 2015, **44**, 15557–15566.